

Stiffness of Contacts Between Rough Surfaces

Sreekanth Akarapu, Tristan Sharp and Mark O. Robbins¹

¹*Department of Physics and Astronomy, Johns Hopkins University,
3400 N Charles St, Baltimore, MD 21218, USA*

(Dated: December 30, 2019)

The effect of self-affine roughness on solid contact is examined with molecular dynamics and continuum calculations. The contact area and normal and lateral stiffnesses rise linearly with the applied load, and the load rises exponentially with decreasing separation between surfaces. Results for a wide range of roughnesses, system sizes and Poisson ratios can be collapsed using Persson's contact theory for continuous elastic media. The atomic scale response at the interface between solids has little effect on the area or normal stiffness, but can greatly reduce the lateral stiffness. The scaling of this effect with system size and roughness is discussed.

PACS numbers: 46.55.+d, 62.20.Qp, 81.40.Pq

The presence of roughness on a wide range of length scales has profound effects on contact and friction between experimental surfaces. Under a broad range of conditions [1–6], the area of intimate contact between rough surfaces A_c is orders of magnitude smaller than the apparent surface area A_0 . As discussed below, this provides the most common explanation for Amontons' laws that friction is proportional to load and independent of A_0 . Because A_c is small, the interfacial region is very compliant. In a range of applications the interfacial compliance can significantly reduce the stiffness of macroscopic joints formed by holding two components together under pressure [1, 7].

In this paper, we examine the effect of surface roughness on the normal and lateral stiffness of contacts between elastic solids using molecular dynamics (MD) and continuum calculations. The results provide a numerical test of recent continuum theories [8, 9] and their applicability to real solids. The contact area and normal stiffness approach continuum predictions rapidly as system size increases. Continuum theory also captures the internal deformations in the solid under tangential load, but the total lateral stiffness may be greatly reduced by atomic scale displacements between contacting atoms on the opposing surfaces. This makes it a sensitive probe of the forces underlying friction and may help to explain unexpectedly small experimental results [10].

The topography of many surfaces can be described as a self-affine fractal [2, 11]. Over a wide range of lengths, the root mean squared (rms) change in height dh over a lateral distance ℓ scales as a power law: $dh \sim \ell^H$, where the roughness or Hurst exponent H is typically between 0.5 and 0.9. Greenwood and Williamson (GW) considered the peaks of rough landscapes as independent asperities and found that A_c rose linearly with normal load F_N for nonadhesive surfaces [2]. This explains Amontons' laws if there is a constant shear stress at the interface. A linear scaling of area with load is also obtained from Persson's scaling theory, which includes elastic coupling between contacts approximately [12, 13].

Dimensional analysis implies that the linear relation between load and area must have the form

$$A_c E' = \kappa F_N / \sqrt{|\nabla h|^2}. \quad (1)$$

where a modulus like the contact modulus E' is the only dimensional quantity characterizing the elastic response, and the rms slope the only dimensionless quantity characterizing the roughness. Numerical solutions of the continuum equations [4, 6] show that κ is near 2. Results for different H and Poisson ratio ν lie between the analytic predictions of GW, $\sqrt{2\pi} \sim 2.5$, and Persson, $\sqrt{8/\pi} \sim 1.6$. One advantage of Persson's model is that, as in numerical results, A_c/F_N is constant over a much larger range of loads than GW [14]. Another is that it captures [9] the power law scaling of correlations in contact and stress that was found in numerical studies [15, 16].

The normal stiffness is related to the change in average surface separation u with load. Experiments [17, 18] and calculations [5, 8, 19] show an exponential rise in load with decreasing u , $F_N = cA_0 E' \exp[-u/\gamma h_{\text{rms}}]$, where h_{rms} is the root mean squared (rms) variation in surface height and γ a constant of order 1. Differentiating leads to an expression for the normal interfacial stiffness:

$$k_N^I = -dF_N/du = F_N/\gamma h_{\text{rms}}. \quad (2)$$

For self-affine surfaces this interfacial stiffness decreases as $h_{\text{rms}}^{-1} \sim L^{-H}$ with increasing system size L . Our simulations test this scaling and show that γ is nearly constant. They also examine the connection between this normal stiffness and the transverse stiffness k_T^I at forces lower than the static friction [20].

We consider nonadhesive contact of a rigid rough solid and a flat elastic substrate. This can be mapped to contact of two rough, elastic solids in continuum theories [2, 12]. The mapping is only approximate for atomic systems [21, 22], but working with one rigid solid reduces the parameter space in this initial study. Rigid surface atoms are placed on the sites of a simple cubic lattice with spacing d' , and only atoms in the outer layer are

close enough to interact with the substrate. They are displaced vertically to coincide with a self-affine fractal surface of the desired H . Surfaces with roughness on wavelengths from l_{\min} to l_{\max} were generated as in Ref. [15]. The rms slope $\sqrt{|\nabla h|^2} = 0.1$ for the results shown. Consistent results were obtained for slopes from 0.05 to 0.15. Slopes of 0.2 or greater led to plastic deformation in the substrate. Continuum calculations also show plasticity for large slopes [5].

The elastic substrate is an fcc crystal with nearest-neighbor spacing d and a (100) surface. Surface atoms form a square lattice that is rotated by 45° relative to that of the rigid surface. This rotation and the choice of d/d' prevent commensurate locking of the surfaces [23, 24]. Substrate atoms separated by r interact with a Lennard-Jones (LJ) potential: $U_{LJ} = 4\epsilon[(\sigma/r)^{12} - (\sigma/r)^6]$, where ϵ and σ are the bonding energy and diameter. To speed calculations, the potential and force are interpolated smoothly to zero at $r_c = 1.8\sigma$ [25]. Since we compare to continuum theories with no interfacial adhesion, purely repulsive interactions are used between substrate and rigid atoms. An LJ potential with length σ' is truncated at the energy minimum, $2^{1/6}\sigma'$. Unless noted $\sigma' = 0.5\sigma$ and $d' = 0.3d$ to minimize interfacial friction and speed the approach to continuum theory [6].

Substrate atoms are arranged to form a cube of side L . Periodic boundary conditions are applied in the plane of the surface and bottom atoms are held fixed. The elastic constants $c_{33} = 70.2\epsilon/\sigma^3$ and $c_{44} = 41.8\epsilon/\sigma^3$ were measured by displacing the top surface. Cubic crystals do not exhibit the isotropic elasticity assumed in continuum theory. To test for any effect from anisotropy, we also performed Greens function MD (GFMD) [26] for isotropic continua with $\nu = 0$ and 0.35. Since thermal fluctuations are ignored in continuum theory, we consider the limit of zero temperature T . The energy is minimized for given external forces or displacements. The fractional contact area A_c/A_0 is obtained from the fraction of surface atoms that interact with the rigid surface [21].

In all cases studied, A_c rises linearly with F_N . Moreover, the value of κ approaches previous continuum results as system size increases. The decrease in κ with increasing L is similar to that found by Campana and Müser in their GFMD calculations [6]. We found κ converged more rapidly when their atomistic Greens function was replaced by an ideal elastic Greens function and we use this in the GFMD results below. As in previous 2D atomistic calculations [21], the stress and contact correlation functions from our LJ calculations exhibited the power law scaling $q^{-(1+H)}$ found in GFMD calculations and Persson's theory [9, 16].

Figure 1 shows the variation of F_N with interfacial separation u for several L and $H = 0.5$ and 0.8. In all cases, F_N rises exponentially over a range of loads that corresponds to fractional contact areas between 1 and 10%. Statistics are too poor at lower areas and non-

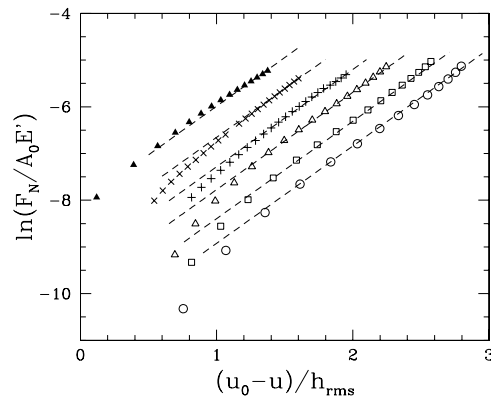


FIG. 1: Logarithm of load as a function of $(u_0 - u)/h_{\text{rms}}$, and linear fits corresponding to $\gamma = 0.48$. The separation at first contact, u_0 , is shifted slightly to prevent overlap. Atomistic results are for $H = 0.5$ with $L = 378.4\sigma$ (circles), 189.2σ (squares), and 94.6σ (triangles) and for $H = 0.8$ with $L = 189.2\sigma$ (crosses) and 94.6σ (pluses). Filled triangles are for a GFMD simulation with $L = 128d$ and $\nu = 0$.

linear corrections to Eq. 1 are seen at larger areas [4]. The linear fits to all results have the same slope, corresponding to $\gamma = 0.48$ and best fit values for all H and L studied differ by less than 10% from this value. GFMD results were at the higher end of this range and showed no change as ν increased from 0 to 0.35. Earlier continuum calculations [5], elastic atomic calculations [19] and experiments [18] were consistent with $\gamma \approx 0.4$. This represents a compelling success of Persson's approach, and raises the question of whether γ may have a unique value in the thermodynamic, isotropic limit.

The normal stiffness from Eq. 2 includes a component from the increase in contact area with load as well as the change in force at fixed area. There is also a compliance associated with changes in the separation between contacting rigid and substrate atoms that is generally neglected in continuum theory. To isolate the stiffness associated with deformation within the substrate at fixed contact area $k^I s$, we applied constraints directly to the atoms that contacted at a given load. The normal and lateral stiffness were then obtained by displacing these contacting atoms in the normal or lateral direction and measuring the change in force. The contribution from the bulk response was subtracted so that the stiffness reflects the change in surface separation u or lateral surface translation u_T . This approach is straightforward to implement in experiments and was found to be consistent with direct averaging of atomic separations.

Figure 2(a) shows the scaled normal interfacial stiffness $k_N^I s h_{\text{rms}}/A_0 E'$ as a function of the dimensionless load $F_N/A_0 E'$ used to find the contacting atoms. Once again, results for all systems show the same behavior, and the stiffness rises linearly with load as predicted by Eq. 2. The points lie slightly above the dashed line corresponding to $\gamma = 0.48$ due to small deviations from the

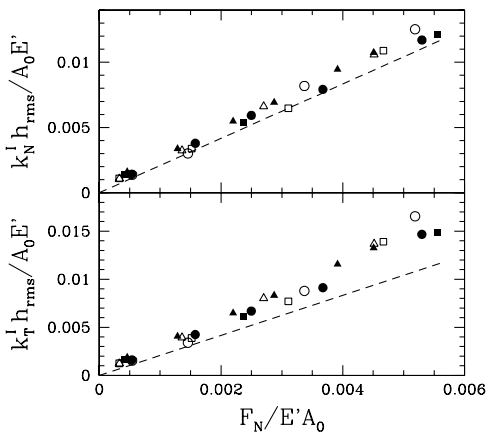


FIG. 2: The scaled (a) normal stiffness and (b) tangential stiffness as a function of $W/A_0 E^*$. Results are for $H = 0.5$ (open symbols) and $H = 0.8$ (filled symbols) with $L = 189.2\sigma$ (circles), $L = 94.6\sigma$ (squares) or $L = 47.3\sigma$ (triangles). Dashed lines have slope $1/\gamma$ with $\gamma = 0.48$.

analytic form of Eq. 2. One might expect k_N^{Is} to be substantially less than the total stiffness because it does not include the stiffness from increases in contact area. However, the two stiffnesses are nearly the same because newly contacting regions carry the smallest forces.

The incremental response of an ideal elastic solid does not depend on any pre-existing deformation. This implies that we should obtain the same stiffness by displacing the same set of atoms on the initial undeformed surface. Direct evaluation of the stiffness in this way gave slightly lower stiffnesses than Fig. 2, with the difference increasing from the numerical uncertainty to about 15% with increasing F_N . This provides an estimate of the contribution that anharmonic effects may make to the stiffness of real materials at the rms slope used here.

The above results imply that the stiffness of elastic solids at fixed contact area is uniquely determined by the distribution of contacting points. This conclusion may seem at odds with Eq. 2, since the contact area has no independent connection to load or surface roughness. The resolution is that variations in load and roughness cancel. If the response is linear, one can scale h_{rms} and F_N by the same factor and the contact area will be unchanged. Indeed one can combine Eqs. 1 and 2 to eliminate F_N :

$$k_N^* \equiv \frac{k_N^I}{A_0 E'} \frac{h_{\text{rms}}}{\sqrt{|\nabla h|^2}} = \frac{1}{\kappa \gamma} \frac{A_c}{A_0}. \quad (3)$$

For a self-affine surface, the ratio $h_{\text{rms}}/\sqrt{|\nabla h|^2} \propto (l_{\text{max}}/l_{\text{min}})^H l_{\text{min}}$ depends only on the small and large scale cutoffs in roughness.

Figure 3(a) shows the scaled stiffness k_N^* vs. area. The results were obtained by displacing atoms from their positions on the initial flat surface to eliminate anharmonic effects. Results for all systems collapse onto a common

straight line, providing clear evidence for the direct connection between stiffness and contacting area. The slope is near unity as expected from the separate values of κ and γ .

All of our atomic simulations show $k_T^{Is}/k_N^{Is} > 1$. This is surprising given that Mindlin [20] and recent work [27] predict $k_T^I/k_N^I = 2(1-\nu)/(2-\nu) < 1$. However, this result is for isotropic systems. One measure of the anisotropy of the LJ crystal is that the ratio $c_{44}/E' \approx 0.57$, while it is $(1-\nu)/2 < 1/2$ for an isotropic solid. This is also consistent with shear stresses having a higher relative stiffness than expected. In general, the total elastic energy stored in the interface is $\Sigma_q \vec{f}(-\vec{q}) G(\vec{q}) \vec{f}(\vec{q})/2$ where G is the Greens function matrix relating displacements to forces f [26]. The ratio of stiffnesses can be obtained by averaging the diagonal components of $qG(\vec{q})$ corresponding to normal and tangential displacements over \hat{q} and assuming the same power spectrum describes the respective forces. This ratio agrees with Mindlin's result for isotropic systems, but will vary with crystal anisotropy.

As noted above, k_N^{Is} and k_T^{Is} only consider the stiffness associated with deformation inside the substrate at constant area. There is an additional stiffness k^{Ia} associated with relative motion at the interface between contacting substrate atoms and the rigid surface. Simulations of single asperity contacts show that this atomic scale motion has very different effects on the total normal and tangential contact stiffness [22]. The stiffness k_N^{Ia} resisting normal displacements is large, because contacting atoms are in the steep repulsive part of the LJ potential. The compliance associated with these bonds has little effect on the total stiffness of single asperities or the multiasperity contacts studied here. As shown above, the full normal stiffness including this compliance and changes in area

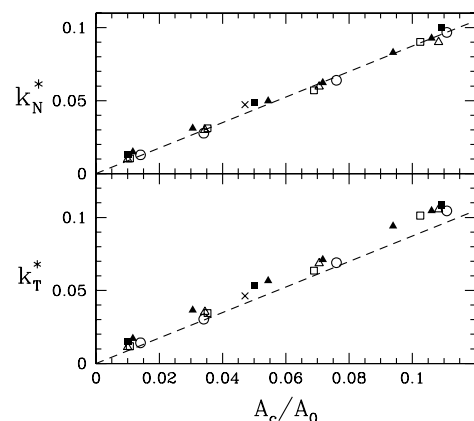


FIG. 3: The scaled (a) normal stiffness and (b) tangential stiffness as a function of A_c/A_0 . Results are for $H = 0.5$ (open symbols) and $H = 0.8$ (filled symbols) with $L = 189.2\sigma$ (circles), $L = 94.6\sigma$ (squares) or $L = 47.3\sigma$ (triangles). Crosses show GFMD results for $\nu = 0$. Dashed lines have slope 0.87.

(Fig. 1) is consistent with the stiffness from compression of the elastic substrate alone (Fig. 2).

In contrast, the tangential stiffness of single asperity contacts can be an order of magnitude or more smaller than continuum predictions [22]. Surfaces rarely share a common period, and the force per area preventing lateral motion averages to zero as the contact size grows [23, 24]. In our simulations, k_T^I depends strongly on d'/d , σ'/σ , l_{\min} , and the orientations of the solids, and the total lateral stiffness is generally too small to distinguish on the scale of Fig. 2. Indeed, this is desirable in comparing to continuum theories for normal contact since they assume zero friction and lateral stiffness.

Our results for a wide range of parameters can be summarized by noting that Eq. 1 arises because the distributions of pressure and contact sizes are independent of load. This implies $k_T^I = \alpha A_c c_{44}/\sigma$ where α is of order one if the contact has the same stiffness as the substrate. Since compliances add, the total interfacial compliance is $1/k_T^I = 1/k_T^A + 1/k_T^S$. Both contributions diverge as F_N and A_c go to zero, explaining why $1/k_T^I$ can be comparable to the bulk compliance of the bounding solids [1, 7]. Since both contributions scale with area, $k_T^I \propto A_c$ but with a lower slope than in Fig. 3.

The substrate compliance dominates for sufficiently large systems and roughness since $k_T^A/k_T^S = \alpha c_{44} h_{\text{rms}}/\sigma E' \sqrt{|\nabla h|^2} \sim (l_{\max}/l_{\min})^H$. However, for small α , the value of l_{\max} required to reach this limit may be large, particularly on the scale of atomistic simulations, microelectromechanical systems, or the wavelength of ultrasound used to measure shear stiffness [10]. For the case of $H = 0.5$ in Fig. 3, k_T^A still reduces the total interfacial stiffness by a factor of two for $l_{\max} \sim 1300\sigma \sim 400\text{nm}$ with $\alpha = 0.1$ and for $l_{\max} \sim 40\mu\text{m}$ for $\alpha = 0.01$. Our measured α span this range and one can estimate α in experimental systems from the static friction coefficient μ_s . If $\beta\sigma$ is the lateral displacement for the force to reach the static friction, then the above equations yield $\alpha = \mu_s \sqrt{|\nabla h|^2}/\kappa\beta$. Typical values of β are of order 1/4 so α and μ are of the same order.

In conclusion, atomic scale simulations were used to study contact between surfaces with roughness on a wide range of scales. The results for area and normal stiffness are consistent with Persson's continuum theory down to relatively small scales even though the solid is not continuous or perfectly elastic. The area and internal stiffnesses of systems with a range of H , L and ν show the linear scaling predicted in Eqs. 1 - 3 with nearly constant values of κ and γ . The internal stiffnesses were shown to depend only on the geometry of the contacting region. Atomic scale displacements between contacting atoms have little effect on the normal stiffness, but can change the lateral

stiffness by orders of magnitude. This sensitivity makes lateral stiffness a promising probe of the atomic scale interactions that underly friction.

Conversations with Martin Müser and Bo Persson are gratefully acknowledged. This material is based upon work supported by the Air Force Office of Scientific Research under Grant No. FA9550-0910232.

-
- [1] F. P. Bowden and D. Tabor, *The Friction and Lubrication of Solids* (Clarendon Press, Oxford, 1986).
 - [2] J. A. Greenwood and J. B. P. Williamson, Proc. R. Soc. London, Ser. A **295**, 300 (1966).
 - [3] B. N. J. Persson, Phys. Rev. Lett. **87**, 116101 (2001).
 - [4] S. Hyun, L. Pei, J.-F. Molinari, and M. O. Robbins, Phys. Rev. E **70**, 026117 (2004).
 - [5] L. Pei, S. Hyun, J.-F. Molinari, and M. O. Robbins, J. Mech. Phys. Sol. **53**, 2385 (2005).
 - [6] C. Campañá and M. H. Müser, Europhys. Lett. **77**, 38005 (2007).
 - [7] D. G. Bellow and D. D. Nelson, Exp. Mech. **10**, 506 (1970).
 - [8] B. N. J. Persson, Phys. Rev. Lett. **99**, 125502 (2007).
 - [9] B. N. J. Persson, J. Phys.: Condens. Matter **20**, 312001 (2008).
 - [10] M. Gonzalez-Valadez, A. Baltazar, and R. S. Dwyer-Joyce, Wear **268**, 373 (2010).
 - [11] J. F. Archard, Proc. R. Soc. London A **243**, 190 (1957).
 - [12] B. N. J. Persson and P. Ballone, J. Chem. Phys. **112**, 9524 (2000).
 - [13] M. H. Müser, Phys. Rev. Lett. **100**, 055504 (2008).
 - [14] G. Carbone and F. Bottigione, J. Mech. Phys. Sol. **56**, 2555 (2008).
 - [15] S. Hyun and M. O. Robbins, Tribol. Int. **40**, 1413 (2007).
 - [16] C. Campañá, M. H. Müser, and M. O. Robbins, J. Phys.: Condens. Matter **20**, 354013 (2008).
 - [17] M. Benz, K. J. Rosenberg, E. J. Kramer, and J. N. Israelachvili, J. Phys. Chem. B **110**, 11884 (2005).
 - [18] B. Lorenz and B. N. J. Persson, **21**, 015003 (2009).
 - [19] C. Yang and B. N. J. Persson, Phys. Rev. Lett. **100**, 024303 (2008).
 - [20] R. D. Mindlin, J. App. Mech. **16**, 259 (1949).
 - [21] B. Luan and M. O. Robbins, Tribol. Lett. **36**, 1 (2009).
 - [22] B. Luan and M. O. Robbins, Nature **435**, 929 (2005), Phys. Rev. E **74**, 026111 (2006).
 - [23] M. Hirano and K. Shinjo, Wear **168**, 121 (1993).
 - [24] M. H. Müser, L. Wenning, and M. O. Robbins, Phys. Rev. Lett. **86**, 1295 (2001).
 - [25] Simulations performed with LAMMPS <http://www.cs.sandia.gov/~sjplimp/lammps.html>.
 - [26] C. Campañá and M. H. Müser, Phys. Rev. B **74**, 075420 (2006).
 - [27] C. Campañá, B. N. J. Persson, and M. H. Müser, private communication.